Measurement of Two-Particle Correlations of Hadrons in e^+e^- Collisions at Belle

Y.-C. Chen[59,*] Y.-J. Lee[59,*] P. Chang,[59] I. Adachi,[19,16] H. Aihara,[84] S. Al Said,[78,39] D. M. Asner,[3] T. Aushev,[21] R. Ayad,[78] V. Babu,[8] P. Behera,[27] K. Belous,[30] J. Bennett,[52] M. Bessner,[18] T. Bilka,[5] D. Bodrov,[21,44] J. Borah,[25] M. Bračko,[49,36] P. Branchini,[32] T. E. Browder,[18] A. Budano,[32] M. Campajola,[31,56] D. Červenkov,[5] M.-C. Chang,[12] V. Chekelian,[50] B. G. Cheon,[17] K. Chilikin,[44] H. E. Cho,[17] K. Cho,[41] S.-J. Cho,[88] S.-K. Choi,[6] Y. Choi,[76] D. Cinabro,[87] S. Das,[48] G. De Nardo,[31,56] G. De Pietro,[32] R. Dhamija,[26] F. Di Capua,[31,56] J. Dingfelder,[2] T. V. Dong,[10] D. Dossett,[51] D. Epifanov,[4,62] T. Ferber,[8] B. G. Fulsom,[64] R. Garg,[65] V. Gaur,[86] A. Giri,[26] P. Goldenzweig,[37] T. Gu,[66] K. Gudkova,[4,62] C. Hadjivasiliou,[64] O. Hartbrich,[18] K. Hayasaka,[61] H. Hayashii,[57] W.-S. Hou,[59] C.-L. Hsu,[77] T. Iijima,[55,54] K. Inami,[54] A. Ishikawa,[19,16] R. Itoh,[19,16] M. Iwasaki,[63] Y. Iwasaki,[19] W. W. Jacobs,[28] S. Jia,[13] Y. Jin,[84] A. B. Kaliyar,[79] C. H. Kim,[17] D. Y. Kim,[75] K.-H. Kim,[88] Y.-K. Kim,[88] P. Kodyš,[5] T. Konno,[40] A. Korobov,[4,62] S. Korpar,[49,36] E. Kovalenko,[4,62] P. Križan,[45,36] R. Kroeger,[52] P. Krokovny,[4,62] M. Kumar,[48] R. Kumar,[67] K. Kumara,[87] A. Kuzmin,[4,62,44] Y.-J. Kwon,[88] Y.-T. Lai,[38] T. Lam,[86] J. S. Lange,[14] M. Laurenza,[32,71] S. C. Lee,[43] J. Li,[43] Y. Li,[13] Y. B. Li,[13] L. Li Gioi,[50] J. Libby,[27] K. Lieret,[46] C.-W. Lin,[59] D. Liventsev,[87,19] A. Martini,[89] M. Masuda,[83,68] T. Matsuda,[53] D. Matvienko,[4,62,44] F. Meier,[9] M. Merola,[31,56] F. Metzner,[37] K. Miyabayashi,[57] G. B. Mohanty,[79] T. J. Moon,[73] R. Mussa,[33] M. Nakao,[19,16] A. Natochii,[18] L. Nayak,[26] N. K. Nisar,[3] S. Nishida,[19,16] K. Nishimura,[18] S. Ogawa,[81] H. Ono,[60,61] G. Pakhlova,[21,44] T. Pang,[66] S. Pardi,[31] S.-H. Park,[19] S. Patra,[24] S. Paul,[80,50] T. K. Pedlar,[47] L. E. Piilonen,[86] T. Podobnik,[45,36] E. Prencipe,[22] M. T. Prim,[2] N. Rout,[27] G. Russo,[56] D. Sahoo,[34] S. Sandilya,[26] A. Sangal,[7] L. Santelj,[45,36] T. Sanuki,[82] V. Savinov,[66] G. Schnell,[1,23] C. Schwanda,[29] R. Seidl,[70] Y. Seino,[61] M. E. Sevior,[51] M. Shapkin,[30] J.-G. Shiu,[59] J. B. Singh,[65,†] A. Sokolov,[30] E. Solovieva,[44] M. Starič,[36] Z. S. Stottler,[86] M. Sumihama,[15] K. Sumisawa,[19,16] W. Sutcliffe,[2] M. Takizawa,[74,20,69] U. Tamponi,[33] K. Tanida,[35] F. Tenchini,[8] M. Uchida,[85] T. Uglov,[44,21] Y. Unno,[17] K. Uno,[61] S. Uno,[19,16] R. Van Tonder,[2] G. Varner,[18] A. Vinokurova,[4,62] A. Vossen,[9] E. Waheed,[19] C. H. Wang,[58] D. Wang,[11] E. Wang,[66] X. L. Wang,[13] S. Watanuki,[88] E. Won,[42] W. Yan,[72] S. B. Yang,[42] H. Ye,[8] J. Yelton,[11] Y. Zhai,[34] Z. P. Zhang,[72] V. Zhilich,[4,62] and V. Zhukova[44]

(Belle Collaboration)

[1]*Department of Physics, University of the Basque Country UPV/EHU, 48080 Bilbao*
[2]*University of Bonn, 53115 Bonn*
[3]*Brookhaven National Laboratory, Upton, New York 11973*
[4]*Budker Institute of Nuclear Physics SB RAS, Novosibirsk 630090*
[5]*Faculty of Mathematics and Physics, Charles University, 121 16 Prague*
[6]*Chung-Ang University, Seoul 06974*
[7]*University of Cincinnati, Cincinnati, Ohio 45221*
[8]*Deutsches Elektronen–Synchrotron, 22607 Hamburg*
[9]*Duke University, Durham, North Carolina 27708*
[10]*Institute of Theoretical and Applied Research (ITAR), Duy Tan University, Hanoi 100000*
[11]*University of Florida, Gainesville, Florida 32611*
[12]*Department of Physics, Fu Jen Catholic University, Taipei 24205*
[13]*Key Laboratory of Nuclear Physics and Ion-beam Application (MOE) and Institute of Modern Physics,*
Fudan University, Shanghai 200443
[14]*Justus-Liebig-Universität Gießen, 35392 Gießen*
[15]*Gifu University, Gifu 501-1193*
[16]*SOKENDAI (The Graduate University for Advanced Studies), Hayama 240-0193*
[17]*Department of Physics and Institute of Natural Sciences, Hanyang University, Seoul 04763*
[18]*University of Hawaii, Honolulu, Hawaii 96822*
[19]*High Energy Accelerator Research Organization (KEK), Tsukuba 305-0801*
[20]*J-PARC Branch, KEK Theory Center, High Energy Accelerator Research Organization (KEK), Tsukuba 305-0801*
[21]*National Research University Higher School of Economics, Moscow 101000*
[22]*Forschungszentrum Jülich, 52425 Jülich*
[23]*IKERBASQUE, Basque Foundation for Science, 48013 Bilbao*
[24]*Indian Institute of Science Education and Research Mohali, SAS Nagar, 140306*
[25]*Indian Institute of Technology Guwahati, Assam 781039*
[26]*Indian Institute of Technology Hyderabad, Telangana 502285*
[27]*Indian Institute of Technology Madras, Chennai 600036*

[28]*Indiana University, Bloomington, Indiana 47408*
[29]*Institute of High Energy Physics, Vienna 1050*
[30]*Institute for High Energy Physics, Protvino 142281*
[31]*INFN - Sezione di Napoli, I-80126 Napoli*
[32]*INFN - Sezione di Roma Tre, I-00146 Roma*
[33]*INFN - Sezione di Torino, I-10125 Torino*
[34]*Iowa State University, Ames, Iowa 50011*
[35]*Advanced Science Research Center, Japan Atomic Energy Agency, Naka 319-1195*
[36]*J. Stefan Institute, 1000 Ljubljana*
[37]*Institut für Experimentelle Teilchenphysik, Karlsruher Institut für Technologie, 76131 Karlsruhe*
[38]*Kavli Institute for the Physics and Mathematics of the Universe (WPI), University of Tokyo, Kashiwa 277-8583*
[39]*Department of Physics, Faculty of Science, King Abdulaziz University, Jeddah 21589*
[40]*Kitasato University, Sagamihara 252-0373*
[41]*Korea Institute of Science and Technology Information, Daejeon 34141*
[42]*Korea University, Seoul 02841*
[43]*Kyungpook National University, Daegu 41566*
[44]*P.N. Lebedev Physical Institute of the Russian Academy of Sciences, Moscow 119991*
[45]*Faculty of Mathematics and Physics, University of Ljubljana, 1000 Ljubljana*
[46]*Ludwig Maximilians University, 80539 Munich*
[47]*Luther College, Decorah, Iowa 52101*
[48]*Malaviya National Institute of Technology Jaipur, Jaipur 302017*
[49]*Faculty of Chemistry and Chemical Engineering, University of Maribor, 2000 Maribor*
[50]*Max-Planck-Institut für Physik, 80805 München*
[51]*School of Physics, University of Melbourne, Victoria 3010*
[52]*University of Mississippi, University, Mississippi 38677*
[53]*University of Miyazaki, Miyazaki 889-2192*
[54]*Graduate School of Science, Nagoya University, Nagoya 464-8602*
[55]*Kobayashi-Maskawa Institute, Nagoya University, Nagoya 464-8602*
[56]*Università di Napoli Federico II, I-80126 Napoli*
[57]*Nara Women's University, Nara 630-8506*
[58]*National United University, Miao Li 36003*
[59]*Department of Physics, National Taiwan University, Taipei 10617*
[60]*Nippon Dental University, Niigata 951-8580*
[61]*Niigata University, Niigata 950-2181*
[62]*Novosibirsk State University, Novosibirsk 630090*
[63]*Osaka City University, Osaka 558-8585*
[64]*Pacific Northwest National Laboratory, Richland, Washington 99352*
[65]*Panjab University, Chandigarh 160014*
[66]*University of Pittsburgh, Pittsburgh, Pennsylvania 15260*
[67]*Punjab Agricultural University, Ludhiana 141004*
[68]*Research Center for Nuclear Physics, Osaka University, Osaka 567-0047*
[69]*Meson Science Laboratory, Cluster for Pioneering Research, RIKEN, Saitama 351-0198*
[70]*RIKEN BNL Research Center, Upton, New York 11973*
[71]*Dipartimento di Matematica e Fisica, Università di Roma Tre, I-00146 Roma*
[72]*Department of Modern Physics and State Key Laboratory of Particle Detection and Electronics, University of Science and Technology of China, Hefei 230026*
[73]*Seoul National University, Seoul 08826*
[74]*Showa Pharmaceutical University, Tokyo 194-8543*
[75]*Soongsil University, Seoul 06978*
[76]*Sungkyunkwan University, Suwon 16419*
[77]*School of Physics, University of Sydney, New South Wales 2006*
[78]*Department of Physics, Faculty of Science, University of Tabuk, Tabuk 71451*
[79]*Tata Institute of Fundamental Research, Mumbai 400005*
[80]*Department of Physics, Technische Universität München, 85748 Garching*
[81]*Toho University, Funabashi 274-8510*
[82]*Department of Physics, Tohoku University, Sendai 980-8578*
[83]*Earthquake Research Institute, University of Tokyo, Tokyo 113-0032*
[84]*Department of Physics, University of Tokyo, Tokyo 113-0033*
[85]*Tokyo Institute of Technology, Tokyo 152-8550*
[86]*Virginia Polytechnic Institute and State University, Blacksburg, Virginia 24061*

[87]*Wayne State University, Detroit, Michigan 48202*
[88]*Yonsei University, Seoul 03722*
[89]*Deutsches Elektronen-Synchrotron, 22607 Hamburg*

The measurement of two-particle angular correlation functions in high-multiplicity e^+e^- collisions at $\sqrt{s} = 10.52$ GeV is reported. In this study, the 89.5 fb^{-1} of hadronic e^+e^- annihilation data collected by the Belle detector at KEKB are used. Two-particle angular correlation functions are measured in the full relative azimuthal angle ($\Delta\phi$) and three units of pseudorapidity ($\Delta\eta$), defined by either the electron beam axis or the event-shape thrust axis, and are studied as a function of charged-particle multiplicity. The measurement in the thrust axis analysis, with mostly outgoing quark pairs determining the reference axis, is sensitive to the region of additional soft gluon emissions. No significant anisotropic collective behavior is observed with either coordinate analyses. Near-side jet correlations appear to be absent in the thrust axis analysis. The measurements are compared to predictions from various event generators and are expected to provide new constraints to the phenomenological models in the low-energy regime.

Two-particle angular correlations have been extensively studied in search of quark-gluon plasma (QGP) formation and its properties in nucleus-nucleus collisions [1–4] over the last several decades. In such collisions, a ridgelike structure of the correlation function, residing in a particular phase space where particle pairs have large differences in pseudorapidity but small differences in azimuthal angle, is observed. This signal in relativistic heavy ion collisions is interpreted as the macroscopic consequence of the hydrodynamical expansion of the perfect-fluid-like QGP state with the presence of initial density fluctuations [5–7]. The ridgelike signal was also observed in high charged-particle multiplicity events in proton-proton, proton-nucleus, deuteron-nucleus, and helium-nucleus collisions [8–16]. Recently, data on ultraperipheral PbPb photonuclear collisions [17] also resulted in significant second-order and third-order flow coefficients, which is an approach to quantify the two-particle azimuthal anisotropy with Fourier harmonics. Essentially, the ridgelike signal is reported in all collision systems involving at least one hadron. However, the physical origin of azimuthal anisotropies in these smaller collision systems is not yet fully understood [18,19]. In hadron-hadron collisions, the complexity introduced by the initial state cannot be easily factored out. A large number of theoretical models based on different underlying mechanisms such as partonic initial-state correlations [20], final-state interactions [21,22], and hydrodynamic medium expansion [23] have been proposed to explain the observed ridgelike signal in these small systems.

To break down the question, high charged-particle multiplicity events produced in even smaller electron-ion and electron-positron (e^+e^-) collisions are proposed to provide accessibility to understanding the cause of this special collective behavior [24]. As an example, a color dipole configuration (two color strings aligned in parallel with a gap in between) in e^+e^- collisions can exhibit anisotropy in the initial parton geometry and generate ridgelike correlations. More importantly, without the presence of initial-state color objects, the study of e^+e^- collisions is a null test for the color glass condensates framework [20,25,26], which attributes collectivity to correlations from the initial-state color field. Recently, experimental studies have been extended to such smaller collision systems, e.g., electron-proton [27] and e^+e^- [28] collisions. No significant ridgelike signal was observed in these measurements. These results have stimulated discussions on the ways to search for and understand possible collectivity signatures in e^+e^- [29–31] and electron-ion collisions [32,33]. However, the data samples used for the search in the e^+e^- ALEPH archived data [28] is small, which motivates the examination of a high-statistics data to study the highest multiplicity tail at Belle.

Taking advantage of the clean environment in e^+e^- collisions and high-statistics data collected with the Belle detector at KEKB [34], the analysis is performed for the first time at a center-of-mass energy of $\sqrt{s} = 10.52$ GeV, which is 60 MeV lower than the $\Upsilon(4S)$ resonance. Overall, a data sample of 89.5 fb^{-1} is utilized in this analysis, which is the full dataset of collisions at $\sqrt{s} = 10.52$ GeV. This analysis closely follows the previous analysis procedure with ALEPH archived data [28]. Although the average event multiplicity is lower than the ALEPH data, the two-particle correlation analysis is performed on the largest off-resonance Belle dataset, whose results can solidify previous findings. The Belle hadronic-event dataset is about 4 times

larger than that with ALEPH archived data, enabling the collectivity search to move forward from a scan among the 0.5% highest multiplicity events of the total distribution to that of 0.02% percentile. Moreover, the measurement of the two-particle correlation function in the low-energy regime can provide additional inputs to the phenomenological fragmentation models.

The Belle detector is a large-solid-angle magnetic spectrometer that consists of a silicon vertex detector, a 50-layer central drift chamber, an array of aerogel threshold Cherenkov counters, a barrel-like arrangement of time-of-flight scintillation counters, and an electromagnetic calorimeter (ECL) comprising CsI(Tl) crystals located inside a superconducting solenoid coil that provides a 1.5 T magnetic field. An iron flux return located outside of the coil is instrumented to detect K_L^0 mesons and muons. The detector is described in detail elsewhere [35].

The hadronic-event selection [36], including requirements on event multiplicity and energy sum in the ECL, is adopted to suppress contamination from two-photon, radiative Bhabha, and other QED events. Particles used in the calculation of the correlation functions are primary charged tracks, defined as prompt tracks or decay products of intermediate particles with proper lifetime $\tau < 1$ cm/c. The corresponding selection on experimental data is tracks produced from the interaction point (including from short-lifetime particle decays) and tracks from long-lifetime particle decays with $V_r < 1$ cm, where V_r is the distance in the transverse plane of the decay vertex from the interaction point. The latter can intersect with other tracks on a common space point and has dihadron invariant mass consistent with the mass of a K_S^0 (0.480–0.516 GeV/c^2) or $\Lambda^0/\bar{\Lambda}^0$ (1.111–1.121 GeV/c^2) candidate; otherwise, the track is deemed as a prompt track and accepted in the primary particle selection. Charged tracks are required to be within the detector acceptance, i.e., with polar angles ranging from 17°–150° (+z is defined opposite to the e^+ beam), and have transverse momenta in the center-of-mass frame greater than 0.2 GeV/c. Impact parameter requirements are adopted to select charged tracks within ±2 cm with respect to the interaction point in the transverse plane, and ±5 cm along the z direction. For a pair of neighboring low-momentum tracks with the absolute value of cosine opening angle greater than 0.95 and transverse momenta below 0.4 GeV/c, the one with less momentum is deemed as a duplicated track and is hence removed. Tracks from photon conversion candidates are vetoed, with the latter selected with the invariant mass less than 0.25 GeV/c^2 and the decay-vertex radius greater than 1.5 cm.

To eliminate the effects of the nonuniform detection efficiency and misreconstruction bias, efficiency correction factors are derived by the Belle Monte Carlo (MC) sample. The Belle MC is simulated based on EvtGen [37] and PYTHIA6 [38], where hadronic $q\bar{q}$ ($q = u$, d, s, c) fragmentation as well as low multiplicity $e^+e^- \to \tau^+\tau^-$ and

TABLE I. Average multiplicities and corrected multiplicities of different $N_{\mathrm{trk}}^{\mathrm{rec}}$ intervals.

$N_{\mathrm{trk}}^{\mathrm{rec}}$ range	Fraction of data (%)	$\langle N_{\mathrm{trk}}^{\mathrm{rec}} \rangle$	$\langle N_{\mathrm{trk}}^{\mathrm{corr}} \rangle$
[6,10)	44.33	6.98	7.05
[10,12)	2.65	10.26	10.12
[12,14)	0.29	12.20	11.90
[14, ∞)	0.02	14.22	14.24

two-photon processes are taken into account. The detector response is simulated with GEANT3 [39]. The MC sample is further reweighted to match event multiplicity and thrust distributions of the data in order to correct for the imperfection in MC simulation. In order to study the multiplicity dependence of the correlation function, the events are binned into multiplicity classes using the reconstructed track multiplicity, denoted $N_{\mathrm{trk}}^{\mathrm{rec}}$, by counting tracks after all selections. For low-multiplicity events with $N_{\mathrm{trk}}^{\mathrm{rec}} < 12$, only a sample size of 11.5 fb^{-1} is used. The multiplicity classes used in this study, their corresponding fraction of data, and the mapping of average reconstructed multiplicities $\langle N_{\mathrm{trk}}^{\mathrm{rec}} \rangle$ to average multiplicities after efficiency correction $\langle N_{\mathrm{trk}}^{\mathrm{corr}} \rangle$ are listed in Table I.

The Belle experiment is operated with the KEKB asymmetric energy collider, colliding the 8 GeV electron beam and the 3.5 GeV positron beam. We boost events to their center-of-mass frame to perform the angular correlation analysis. Following a procedure similar to what has already been established in Ref. [10], the two-particle correlation function observable is defined as

$$\frac{1}{N_{\mathrm{trk}}^{\mathrm{corr}}} \frac{d^2 N^{\mathrm{pair}}}{d\Delta\eta \, d\Delta\phi} = B(0,0) \times \frac{S(\Delta\eta, \Delta\phi)}{B(\Delta\eta, \Delta\phi)}. \quad (1)$$

The correlation function is expressed in terms of the particle pair's angular difference $\Delta\eta = \pm(\eta_i - \eta_j)$ and $\Delta\phi = \pm(\phi_i - \phi_j)$, where i, j label the track pair's indices. The calculation is based on an assumption of correlations being symmetric about the origin $(\Delta\eta, \Delta\phi) = (0,0)$; hence, four entries are counted for a given pair. The per-charged-particle associated track-pair yield is denoted as N^{pair}, and is reweighted by efficiency correction factors of both particles. The signal correlation $S(\Delta\eta, \Delta\phi)$ and the background correlation $B(\Delta\eta, \Delta\phi)$ can be explicitly written out as

$$S(\Delta\eta, \Delta\phi) = \frac{1}{N_{\mathrm{trk}}^{\mathrm{corr}}} \frac{d^2 N^{\mathrm{same}}}{d\Delta\eta \, d\Delta\phi},$$

$$B(\Delta\eta, \Delta\phi) = \frac{1}{N_{\mathrm{trk}}^{\mathrm{corr}}} \frac{d^2 N^{\mathrm{mix}}}{d\Delta\eta \, d\Delta\phi}, \quad (2)$$

where N^{same} (N^{mix}) counts the number of track pairs formed by matching the ith charged particle of a given event with

the jth particle in the same event ("mixed event" [8]). A mixed event in this work is a combination of tracks from three random events and is normalized by a factor of $1/3$. Three random events are chosen such that their $N_{\mathrm{trk}}^{\mathrm{rec}}$'s are the same as that of the event they match to. The $B(0,0)$ factor is incorporated in the calculation of the correlation function, serving as the normalization of the artificially constructed $B(\Delta\eta, \Delta\phi)$. This factor is obtained by extrapolating the function value to the origin of $B(\Delta\eta, \Delta\phi)$. An additional correction on the correlation function is applied to deal with the effects introduced by using finite-bin histogramming to approximate the density function. The bin-size effect is modeled by a second-order polynomial and the magnitude of the correlation function is calibrated. To unfold back to the truth level, final correlations are corrected with the bin-by-bin method [40], accounting for residual reconstruction effects after efficiency corrections.

The two-particle correlation function is explored in two coordinate systems: beam and thrust axis coordinates in the e^+e^- center-of-mass frame. The former is the same as that presented in most of the two-particle correlation studies, while in the latter, initiated by Ref. [28], the event thrust axis [41] is used as the reference axis, with missing momentum of the event included. The construction of mixed events in the thrust axis analysis is identical to that in the beam axis analysis, requiring the multiplicity matching only. In the thrust axis coordinate analysis, the kinematics (p_T, η, ϕ) of a mixed event are calculated with respect to the thrust axis of its matched physical event. To adjust the kinematics distribution of the mixed event to physical kinematic (p_T, η, ϕ) spectra, a reweighting correction is adopted.

In the e^+e^- annihilation process, when the interacting system is located in between or along the color string connecting the $q\bar{q}$ pair, measuring with a coordinate system defined by the event thrust axis provides a more direct picture. From the viewpoint of relativistic fluid dynamics [7], conventional beam-axis measurements are sensitive to features within the plane transverse to the collision axis, probing any anisotropic behavior of the QCD medium, which are widely studied as the phenomena of elliptic or triangular flow [6,42,43]. The insensitive region of the two-particle correlation function in the beam axis analysis is at the beam pipe, where a particle pair with a large pseudorapidity difference is excluded from the finite $\Delta\eta$ region of interest (e.g., $|\Delta\eta| \leq 3.0$ in this analysis). In addition, the on-axis track-pair correlation is too deformed to form an obvious correlation structure, since the ϕ coordinate is ill represented near both poles of the spherical coordinate. Correspondingly, the insensitivity of the thrust-axis correlation function is at its reference thrust axis which quark-initiated dijets are close to; however, they are sensitive in the mid-rapidity region, where additional soft gluons emit apart from the leading quark–antiquark dijetlike structure. The sensitivity to the finer structure allows one to check in
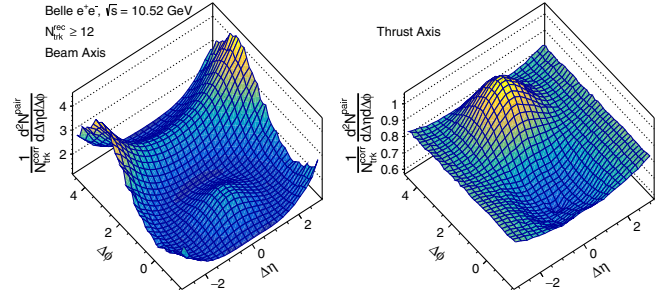

FIG. 1. Two-particle correlation functions for beam (left) and thrust (right) axis analyses with the multiplicity $N_{\mathrm{trk}}^{\mathrm{rec}} \geq 12$.

details if there are special correlations among the color activity in the small system.

In Fig. 1, correlation functions with multiplicity $N_{\mathrm{trk}}^{\mathrm{rec}} \geq 12$ are shown for both beam and thrust axis coordinates. In the beam axis coordinate view, the peak near the origin $(\Delta\eta, \Delta\phi) = (0,0)$ has contributions from pairs originating in the same jet, while the structure at $\Delta\phi \approx \pi$ is from back-to-back correlations. These features reflect the two-particle correlation of dijetlike $q\bar{q}$ events, which mainly contribute in e^+e^- collisions. In contrast, for the thrust axis coordinates, the dominant structure is the hill-like bump near $(\Delta\eta, \Delta\phi) \approx (0, \pi)$, while a sizable near-side correlation is lacking. The decrease of the near-side-peak correlation is because that leading two jets are brought to insensitive regions around poles of the reference thrust axis. As a result of balance for the event thrust calculation, track pairs among on-axis jets tend to yield larger $\Delta\phi$ angular differences. Compared to collisions at high center-of-mass energies, jets are composed of fewer constituents and have broader shapes at the low energy regime. This makes it hard to form a significant near-side-peak correlation. We calculated the magnitude of the near-side-peak correlation with respect to different collision energies with SHERPA2.2.5 [44] simulation of $e^+e^- \rightarrow$ hadrons at the leading order, and found results suggesting a significant correspondence.

Evidence for the ridge signal can be best examined in the azimuthal differential yield $Y(\Delta\phi)$ by averaging the correlation function over the long-range region with $1.5 \leq |\Delta\eta| < 3.0$. A "zero yield at minimum" (ZYAM) method [45] is further implemented to separate any enhanced near-side correlation around $\Delta\phi = 0$ distinct from a constant correlation. The constant contribution along $\Delta\phi$, denoted as C_{ZYAM}, is estimated by the minimum of the fit with a third-order Fourier series to the data points. A fit with a third-order polynomial plus a cosine term, and with a fourth-order polynomial are also checked to estimate C_{ZYAM} in parallel.

The systematic uncertainties due to the selection and correction operations are calculated with respect to long-range $Y(\Delta\phi)$. Hadronic-event selection is examined by tightening the energy sum requirement in the ECL from $E_{\mathrm{sum}} > 0.18\sqrt{s}$ to $0.23\sqrt{s}$. The primary-particle selection

systematic is estimated by making variations of the proper lifetime requirement $\tau < 1\,\mathrm{cm}/c$ and the vertex $V_r < 1$ cm. In general, results from both variations differ by less than 1% (or by 1%–6% for the high-multiplicity bin). A 0.35% uncertainty is quoted for the track reconstruction efficiency, which is evaluated by comparing partially and fully reconstructed $D^* \to \pi_{\mathrm{slow}} D^0[\to \pi^+ \pi^- K_S^0 (\to \pi^+ \pi^-)]$ decays [46]. In the beam axis analysis, the systematic uncertainties are mainly from the primary-particle selection and the tracking efficiency, which are in general on the order of 0.3%–0.4%, while the primary-particle selection increases to a 6.3% uncertainty for high-multiplicity events with $N_{\mathrm{trk}}^{\mathrm{rec}} \geq 14$. For high-multiplicity event classes in the thrust axis analysis, dominant sources of systematic uncertainties are due to the event selection ($< 2\%$) and the primary-particle selection ($< 4\%$), where the estimation of uncertainties suffers from the need for large statistics to derive a precise reweighting factor for the efficiency correction and for the mixed events. On the other hand, for low-multiplicity classes, the dominant source of uncertainty is due to tracking. Other uncertainties originate from MC reweighting, the $B(0, 0)$ factor, mixed events reweighting, scaling corrections due to bin effects and residual bin effects, all of which are checked to be small in different multiplicity bins of order $\mathcal{O}(10^{-4})$, with the largest one contributing up to 0.3% uncertainty.

Figure 2 shows the measurement of long-range $Y(\Delta\phi)$ after performing the ZYAM method, along with a comparison of predictions from Belle MC, HERWIG 7.2.2 [47], and SHERPA 2.2.5 [44] event generators. The latter two use a cluster model for hadronization, while the PYTHIA-based Belle MC is based on the Lund string model. The region with small azimuthal angle difference ($\Delta\phi \approx 0$) is where possible ridge signals would be visible as a nonzero value. In the beam axis coordinates, all generators are consistent with data in the near-side ridge region, but in the away-side region, HERWIG and SHERPA undershoot the data. In the thrust axis analysis, the Belle simulation, with specific tunes adapted to Belle data, gives again a better description of these correlation data. A larger discrepancy from the data is seen in the HERWIG simulation, while SHERPA shows a milder disagreement; there are overpredictions in the away-side region and an excess of correlations in the near-side ridge-prone region. Note that this simulated enhanced structure is different from typical ridge signals, which spread over a wide range of $\Delta\eta$. With the absence of the near-side peak at $\sqrt{s} = 10.52$ GeV, the excess only occurs at the long-range near-side region. This enhancement could come from different modeling in the hadronization or parton shower.

The significance of any ridge signal can be quantified by integrating over $Y(\Delta\phi)$ from $\Delta\phi = 0$ to where the ZYAM fit minimum occurs. Ridge yields smaller than an order of 10^{-10} are measured. Since there is no obvious ridgelike structure in either the beam or thrust axis analysis, a
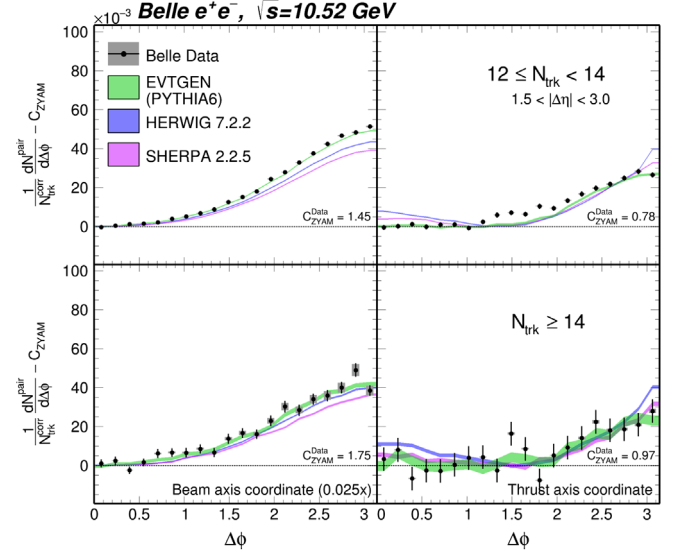

FIG. 2. Comparison of ZYAM-subtracted $Y(\Delta\phi)$ in the range $1.5 \leq |\Delta\eta| < 3.0$ for the multiplicity $12 \leq N_{\mathrm{trk}}^{\mathrm{rec}} < 14$ (top) and $N_{\mathrm{trk}}^{\mathrm{rec}} \geq 14$ (bottom), where subtracted constants of data $C_{\mathrm{ZYAM}}^{\mathrm{Data}}$ are quoted. In each panel, results for beam (left) and thrust (right) axis analyses are displayed. The colored bands show simulation predictions from Belle MC (green), HERWIG (blue), and SHERPA (violet). The error bars on the data represent the statistical uncertainties, and the gray boxes are systematic uncertainties. For visual purposes, the minimal statistical uncertainty of the MC colored bands is set to be 3×10^{-4}, and beam-axis ZYAM-subtracted yields are scaled by a factor of 0.025.

bootstrap procedure [48] is implemented and the confidence limit of the integrated ridge yield is reported. In the bootstrap procedure, each azimuthal differential yield distribution is varied according to their statistical and systematic uncertainties, and the yield distribution is
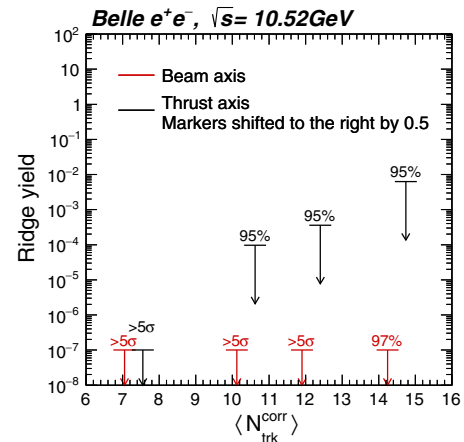

FIG. 3. Upper limits of the ridge yield as a function of $\langle N_{\mathrm{trk}}^{\mathrm{corr}} \rangle$ in beam axis (red) and thrust axis (black) coordinate frames. Thrust axis limits are shifted to the right by 0.5 for presentation purposes. The label "$> 5\sigma$" indicates the 5σ confidence level upper limit.

sampled 2×10^6 times. For the ZYAM subtraction, three fit templates (a third-order Fourier series, a third-order polynomial plus a cosine term, and a fourth-order polynomial) are attempted, of which the most conservative confidence limit is quoted. In Fig. 3, the 95% confidence level upper limits as a function of $\langle N_{\text{trk}}^{\text{corr}} \rangle$ are reported. For the ridge yield upper limit less than 10^{-7}, we report the confidence levels of the ridge signal exclusion, instead.

In summary, the first measurement of two-particle correlations of hadrons in beam and thrust axis coordinate systems, performed using e^+e^- collision data at $\sqrt{s} = 10.52$ GeV from Belle is reported. A strong exclusion of ridge yield in the beam axis coordinate analysis is set. In the thrust axis coordinate analysis, there is no significant near-side-peak correlation, different from what was observed in hadronic collisions or high-energy e^+e^- collisions. A 95%–97% C.L. upper limit or a 5σ exclusion is set versus $\langle N_{\text{trk}}^{\text{corr}} \rangle$ for the absence of any ridge yield in our measurement. Though there is no hint of collectivity signals in the low-energy e^+e^- collision system, the measurement can be provided as a reference for tunes of fragmentation models in the soft QCD scale. Belle MC samples based on EvtGen (with a PYTHIA6 interface for $e^+e^- \to q\bar{q}$ generation), along with HERWIG and SHERPA event generators are examined. Similar to the conclusion from the previous analysis with ALEPH archived data [28], the results in this study are found to be better described by PYTHIA6 than SHERPA or HERWIG.

———————

[*]Present address: Massachusetts Institute of Technology, Cambridge, Massachusetts 02139, USA.

[†]Also at University of Petroleum and Energy Studies, Dehradun 248007.

[1] I. Arsene *et al.* (BRAHMS Collaboration), Nucl. Phys. **A757**, 1 (2005).

[2] B. Back *et al.* (PHOBOS Collaboration), Nucl. Phys. **A757**, 28 (2005).

[3] J. Adams *et al.* (STAR Collaboration), Nucl. Phys. **A757**, 102 (2005).

[4] K. Adcox *et al.* (PHENIX Collaboration), Nucl. Phys. **A757**, 184 (2005).

[5] J.-Y. Ollitrault, Phys. Rev. D **46**, 229 (1992).

[6] B. Alver and G. Roland, Phys. Rev. C **81**, 054905 (2010); **82**, 039903(E) (2010).

[7] U. Heinz and R. Snellings, Annu. Rev. Nucl. Part. Sci. **63**, 123 (2013).

[8] V. Khachatryan *et al.* (CMS Collaboration), J. High Energy Phys. 09 (2010) 091.

[9] G. Aad *et al.* (ATLAS Collaboration), Phys. Rev. Lett. **116**, 172301 (2016).

[10] S. Chatrchyan *et al.* (CMS Collaboration), Phys. Lett. B **718**, 795 (2013).

[11] B. Abelev *et al.* (ALICE Collaboration), Phys. Lett. B **719,** 29 (2013).

[12] G. Aad *et al.* (ATLAS Collaboration), Phys. Rev. Lett. **110,** 182302 (2013).

[13] A. Adare *et al.* (PHENIX Collaboration), Phys. Rev. Lett. **111,** 212301 (2013).

[14] S. Chatrchyan *et al.* (CMS Collaboration), Eur. Phys. J. C **72,** 2012 (2012).

[15] R. Aaij *et al.* (LHCb Collaboration), Phys. Lett. B **762,** 473 (2016).

[16] J. Adam *et al.* (STAR Collaboration), Phys. Rev. Lett. **122,** 172301 (2019).

[17] G. Aad *et al.* (ATLAS Collaboration), Phys. Rev. C **104,** 014903 (2021).

[18] K. Dusling, W. Li, and B. Schenke, Int. J. Mod. Phys. E **25,** 1630002 (2016).

[19] J. L. Nagle and W. A. Zajc, Annu. Rev. Nucl. Part. Sci. **68,** 211 (2018).

[20] K. Dusling and R. Venugopalan, Phys. Rev. D **87,** 094034 (2013).

[21] L. He, T. Edmonds, Z.-W. Lin, F. Liu, D. Molnar, and F. Wang, Phys. Lett. B **753,** 506 (2016).

[22] C. Bierlich, G. Gustafson, and L. Lnnblad, Phys. Lett. B **779,** 58 (2018).

[23] P. Bozek, Phys. Rev. C **85,** 014911 (2012).

[24] J. L. Nagle, R. Belmont, K. Hill, J. O. Koop, D. V. Perepelitsa, P. Yin, Z.-W. Lin, and D. McGlinchey, Phys. Rev. C **97,** 024909 (2018).

[25] F. Gelis, E. Iancu, J. Jalilian-Marian, and R. Venugopalan, Annu. Rev. Nucl. Part. Sci. **60,** 463 (2010).

[26] A. Dumitru, K. Dusling, F. Gelis, J. Jalilian-Marian, T. Lappi, and R. Venugopalan, Phys. Lett. B **697,** 21 (2011).

[27] I. Abt *et al.* (ZEUS Collaboration), J. High Energy Phys. 04 (2020) 070.

[28] A. Badea, A. Baty, P. Chang, G. M. Innocenti, M. Maggi, C. McGinn, M. Peters, T.-A. Sheng, J. Thaler, and Y.-J. Lee, Phys. Rev. Lett. **123,** 212002 (2019).

[29] C. Bierlich, S. Chakraborty, G. Gustafson, and L. Lönnblad, J. High Energy Phys. 03 (2021) 270.

[30] P. Castorina, D. Lanteri, and H. Satz, Eur. Phys. J. A **57,** 111 (2021).

[31] A. Baty, P. Gardner, and W. Li, arXiv:2104.11735.

[32] Y. Shi, L. Wang, S.-Y. Wei, B.-W. Xiao, and L. Zheng, Phys. Rev. D **103,** 054017 (2021).

[33] P. Agostini *et al.* (LHeC, FCC-he Study Group Collaboration), J. Phys. G **48,** 110501 (2021).

[34] S. Kurokawa and E. Kikutani, Nucl. Instrum. Methods Phys. Res., Sect. A **499,** 1 (2003), and other papers included in this Volume; T. Abe *et al.*, Prog. Theor. Exp. Phys. **2013,** 03A001 (2013) and references therein.

[35] A. Abashian *et al.* (Belle Collaboration), Nucl. Instrum. Methods Phys. Res., Sect. A **479,** 117 (2002); also see Section II in J. Brodzicka *et al.*, Prog. Theor. Exp. Phys. **2012,** 04D001 (2012).

[36] K. Abe *et al.* (Belle Collaboration), Phys. Rev. D **64,** 072001 (2001).

[37] A. Ryd *et al.*, Report No. EVTGEN-V00-11-07, 2005.

[38] T. Sjöstrand, P. Edén, C. Friberg, L. Lönnblad, G. Miu, S. Mrenna, and E. Norrbin, Comput. Phys. Commun. **135,** 238 (2001).

[39] R. Brun *et al.*, CERN Report No. DD/EE/84-1, 1984.

[40] G. Choudalakis (ATLAS Collaboration), in *Proceedings of the PHYSTAT 2011 Workshop on Statistical Issues Related to Discovery Claims in Search Experiments and Unfolding* (CERN, Geneva, 2011), 10.5170/CERN-2011-006.297.

[41] E. Farhi, Phys. Rev. Lett. **39,** 1587 (1977).

[42] T. A. Trainor, Phys. Rev. C **81,** 014905 (2010).

[43] K. Aamodt *et al.* (ALICE Collaboration), Phys. Rev. Lett. **105,** 252302 (2010).

[44] E. Bothmann *et al.* (Sherpa Collaboration), SciPost Phys. **7,** 034 (2019).

[45] N. N. Ajitanand, J. M. Alexander, P. Chung, W. G. Holzmann, M. Issah, Roy A. Lacey, A. Shevel, A. Taranenko, and P. Danielewicz, Phys. Rev. C **72,** 011902(R) (2005).

[46] Ed. A. J. Bevan, B. Golob, Th. Mannel, S. Prell, and B. D. Yabsley, Eur. Phys. J. C **74,** 3026 (2014).

[47] J. Bellm *et al.*, Eur. Phys. J. C **76,** 196 (2016).

[48] B. Efron, Ann. Statist. **7,** 1 (1979).